Int. J. Electrochem. Sci., 17 **(2022)** Article Number: 220833, doi: 10.20964/2022.08.24

International Journal of
ELECTROCHEMICAL
SCIENCE
www.electrochemsci.org

Short Communication

Effects of Austenitizing Temperature on Microstructure Evolution and Corrosion Resistance of High Cr Ferritic/Martensitic Steel

Xiaoyu Huang[1,3,4], Heng Wang[1,3,4], Jianguo Chen[2,], Lihua Dang[1,3,4], Zhongqiang Ma[1,3,4], Shibo Cui[1,3,4]*

[1] Tianjin Special Equipment Inspection Institute, Tianjin 300192, PR China;
[2] The 18th Research Institute of China Electronics Technology Group Corporation, Tianjin 300384, PR China;
[3] National Inspection and Detection Center for Special Equipment Welding Consumables Quality, Tianjin 300350, PR China;
[4] Key Laboratory of Digital Twin Generic Technology in Special Equipment for State Market Regulation, Tianjin 300192, PR China;
[*]E-mail: jianguo_chen123@163.com (J. Chen)

Received: 7 May 2022 / *Accepted:* 5 June 2022 / *Published:* 4 July 2022

The effect of austenitizing temperature on microstructure evolution and corrosion resistance of the high Cr ferritic/martensitic steel was studied. The prior austenite grain size, martensite lath width and the size distribution of the second phase (Cr rich carbides) were observed by optical microscope (OM), scanning electron microscope (SEM) and transmission electron microscope (TEM), respectively. The corrosion resistance of the steel was tested by electrochemical polarization curve. The results show that austenitizing temperature can affect the microstructure and corrosion resistance of the high Cr ferritic/martensitic steel. With the increase of austenitizing temperature from 950 ºC to 1100 ºC, the prior austenite grain size and martensite lath width of steel increase. The size of the second phase first decreases and then increases with the increase of austenitizing temperature, while its density first increases and then decreases. The electrochemical polarization curve confirmed that the corrosion current density of the steel first decreases and then increases with the increase of austenitizing temperature, and the corrosion rate showed the same change law as the corrosion current density, indicating that the corrosion resistance of the high Cr ferritic/martensitic steel first enhances and then deteriorates with the increase of austenitizing temperature.

Keywords: High Cr ferritic/martensitic steel; Austenitizing temperature; Carbide; Electrochemical polarization curves, Corrosion rate

1. INTRODUCTION

High Cr ferritic/martensitic steels have been widely used in high-temperature components of

advanced thermal power plants (such as main steam piping, superheater and reheater piping, etc.), owing to their excellent high-temperature durability and creep properties, good thermal conductivity, low thermal expansion coefficient and high ratio of performance to price [1-4]. In addition, high Cr ferritic/martensitic steels are candidates for structural components of nuclear power plants due to their excellent radiation resistance [5]. Ferritic/martensitic steels are usually produced in normalized and tempered conditions, and their microstructure is characterized by a tempered martensitic lath decorated with carbides [6-9]. Therefore, austenitizing process is the first step of heat treatment of forged or hot rolled ferritic/martensitic steels, which plays a decisive role in the microstructure control of steel during heat treatment and the properties after heat treatment [10-12].

The austenitizing temperature has an important influence on the microstructure stability and mechanical properties of ferritic/martensitic steels, due to the changes in the grain size of the prior austenite and the content of dissolved alloying elements in the austenite during austenitizing process [13,14]. Pandey et al. [15] found that as the austenitizing temperature increased to 1100 ^{o}C, the size of the precipitates along the prior austenite grain boundaries and within the grains increased, which would lead to an increase in the tensile strength and a decrease in the toughness of the steel. Yan et al. [16] studied the microstructure and mechanical strength of tempered 9Cr martensitic steels at austenitizing temperature from 900 ^{o}C to 1200 ^{o}C, and found that higher austenitizing temperature leads to the redissolution of coarse-grained carbides, and fine carbide particles are precipitated during tempering. The tensile strength of the steel increases as the austenitizing temperature increases from 900 ^{o}C to 1000 ^{o}C. There is little change in strength from 1000 ^{o}C to 1100 ^{o}C, but continues to increase as the austenitizing temperature rises to 1200 ^{o}C. So far, most studies have focused on the effect of heat treatment on the microstructure and mechanical properties of the high Cr ferritic/martensitic steels. However, there are very few studies on the corrosion properties of the high Cr ferritic/martensitic steel caused by the corresponding microstructure formed during the heat treatment process. Corrosion resistance is the main failure mode of metallic materials, which must be paid attention to [17].

In this paper, the effects of austenitizing temperature on microstructure evolution and corrosion resistance of the high Cr ferrite/martensite steel were systematically investigated by optical microscopy (OM), scanning electron microscope (SEM), transmission electron microscope (TEM) and electrochemical polarization curve. The research results can provide a theoretical basis for the heat treatment of the ferrite/martensite steels in practical engineering.

2. MATERIALS AND EXPERIMENT METHODS

2.1 Specimens preparation

The high Cr ferritic/martensitic steel was smelted into a 28 kg ingot in a vacuum induction furnace, melted twice to ensure the uniformity of its chemical composition and microstructure, and then forged into a cylindrical bar with a height of 350 mm and a diameter of 120 mm. The chemical composition of the experimental steel is given in Table 1. The metallographic structure of the steel is martensite plus a small amount of δ-ferrite, as presented in Fig. 1.

Table 1. Chemical composition of the experimental steel (in wt.%)

C	Cr	W	Mn	Si	V	Ta	Fe
0.04	8.93	1.72	0.44	0.04	0.22	0.07	Bal.

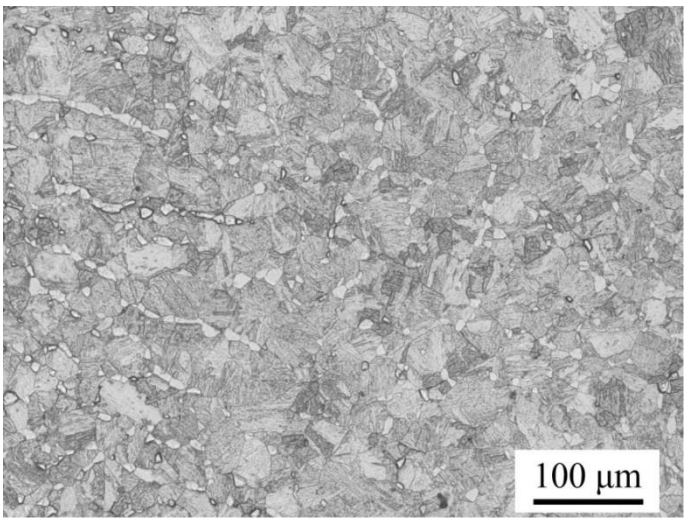

Figure 1. Metallographic structure of the original high Cr ferritic/martensitic steel.

Several 3 cm square samples were cut from the middle of the steel bar, and the heat treatment tests of different processes were carried out on them. Fig. 2 shows the flow-process diagram of the heat treatment experiment for the high Cr ferritic/martensitic steels. The specific process parameters are as follows: the steel blocks were heated from room temperature to 950 ^{o}C, 1000 ^{o}C, 1050 ^{o}C and 1100 ^{o}C at a heating rate of 200 ^{o}C/min, respectively, holding for 20 minutes, and then cooled to room temperature in air. Then, the samples were uniformly tempered at 750 ^{o}C for 90 minutes.

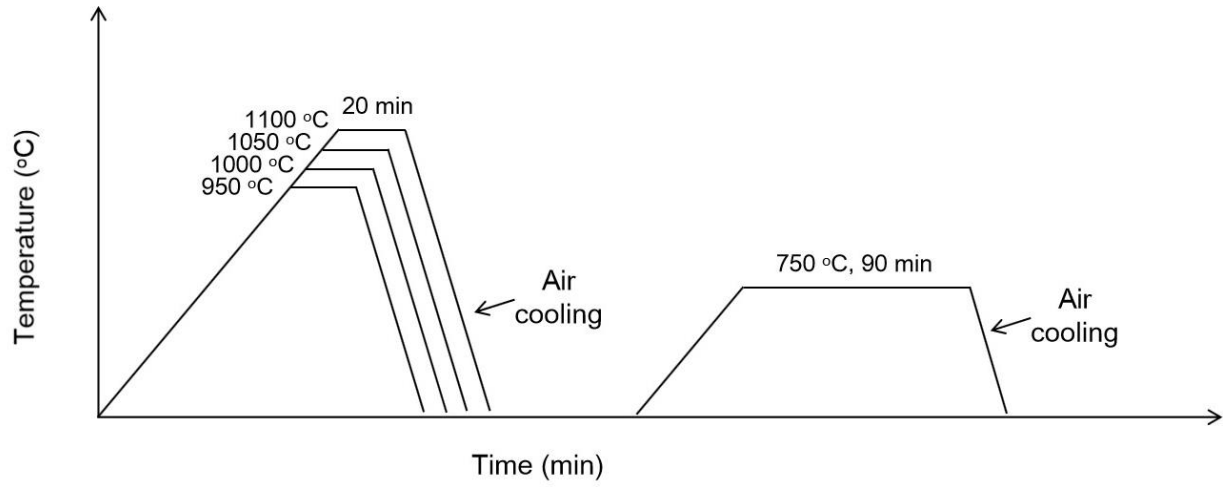

Figure 2. Flow-process diagram of the heat treatment experiment for the high Cr ferritic/martensitic steels.

2.2 Microstructure analysis

The prior austenite grain size of the high Cr ferritic/martensitic steels subjected to the heat treatment was observed by optical microscopy (OM). The samples after the heat treatment experiments were sequentially mounted, ground, polished and etched. When observing the prior austenite grain size, the samples were etched by saturated picric acid solution etching method. The method is to boil the polished metallographic sample in a saturated picric acid solution at 70 ^{o}C for 3 minutes, and then rinse the etched sample with alcohol. The prior austenite grain size of the samples was observed with a Leica DMI 5000m optical microscope. The formula for the picric acid solution is 2 g picric acid + 2 mL cleaning solution + 100 mL water.

The microstructure of the tempered specimens was examined by an S4800 scanning electron microscope (SEM). The polished samples were etched by $FeCl_3$ solution etching method. The formula of $FeCl_3$ solution is 30 mL hydrochloric acid + 100 mL water + 10 g $FeCl_3$.

The distribution of the second phase was observed by transmission electron microscopy (TEM), and the type of the second phase was identified by energy dispersive spectrometer (EDS). When observing martensitic laths, metal thinning samples were used. All samples were cut into 0.3 mm thin slices, and then grind them manually to about 50 μm. Small rounds with a diameter of 3 mm are made with a punch, and then the small piece is thinned on the MTP-1A magnetic-driven double-spray electrolytic thinning instrument. The electrolytic double-spray liquid is a mixture of 5% perchloric acid + 95% alcohol, and the electrolytic voltage and temperature are 40 V and -20 ^{o}C, respectively. Since the second phase in the steel is obscured by diffraction contrast in the metal foil, the morphology, size and distribution of the second phase particles were observed by the carbon extraction replica technique. After deep etching and carbon coating on the surface of the sample, the surface was lightly engraved into a square with a side length of 2 mm, and then soaked in a mixed solution of hydrochloric acid and copper chloride until the carbon film fell off. The small copper mesh was removed, then washed in alcohol and water, and finally dried on filter paper. The samples were observed with a Jem-2100f type transmission electron microscope.

2.3 Electrochemical measurements

The polarization curves of the high Cr ferritic/martensitic steels obtained at different austenitizing temperatures were measured in 3.5 wt.% NaCl solution at room temperature. The acquisition of electrochemical polarization curves was performed on a PARSTAT 4000A electrochemical workstation, which contained a saturated calomel reference electrode, a platinum counter electrode, and a working electrode made from the sample. During the electrochemical polarization curve test, the scan rate was kept at 0.4 mV/s. The surface area of the electrochemical test sample is 1 cm^2.

3. RESULTS AND DISCUSSION

3.1 Microstructure of the high Cr ferritic/martensitic steels

3.1.1 OM observation

Fig. 3 shows the OM micrographs of the high Cr ferritic/martensitic steels subjected to different austenitizing temperatures. It can be found that the prior austenite grains after austenitizing treatment are more uniform compared with the original sample, and the grain morphologies of all the austenitized samples are equiaxed. The prior austenite grain size increases gradually with the increase of austenitizing temperature. This can be explained by the fact that when the austenitizing temperature increases, the second phase particles in the steel are completely dissolved, resulting in the weakening of the pinning effect of the second phase particles on the austenite grain boundaries and promoting the growth of austenite grains [18].

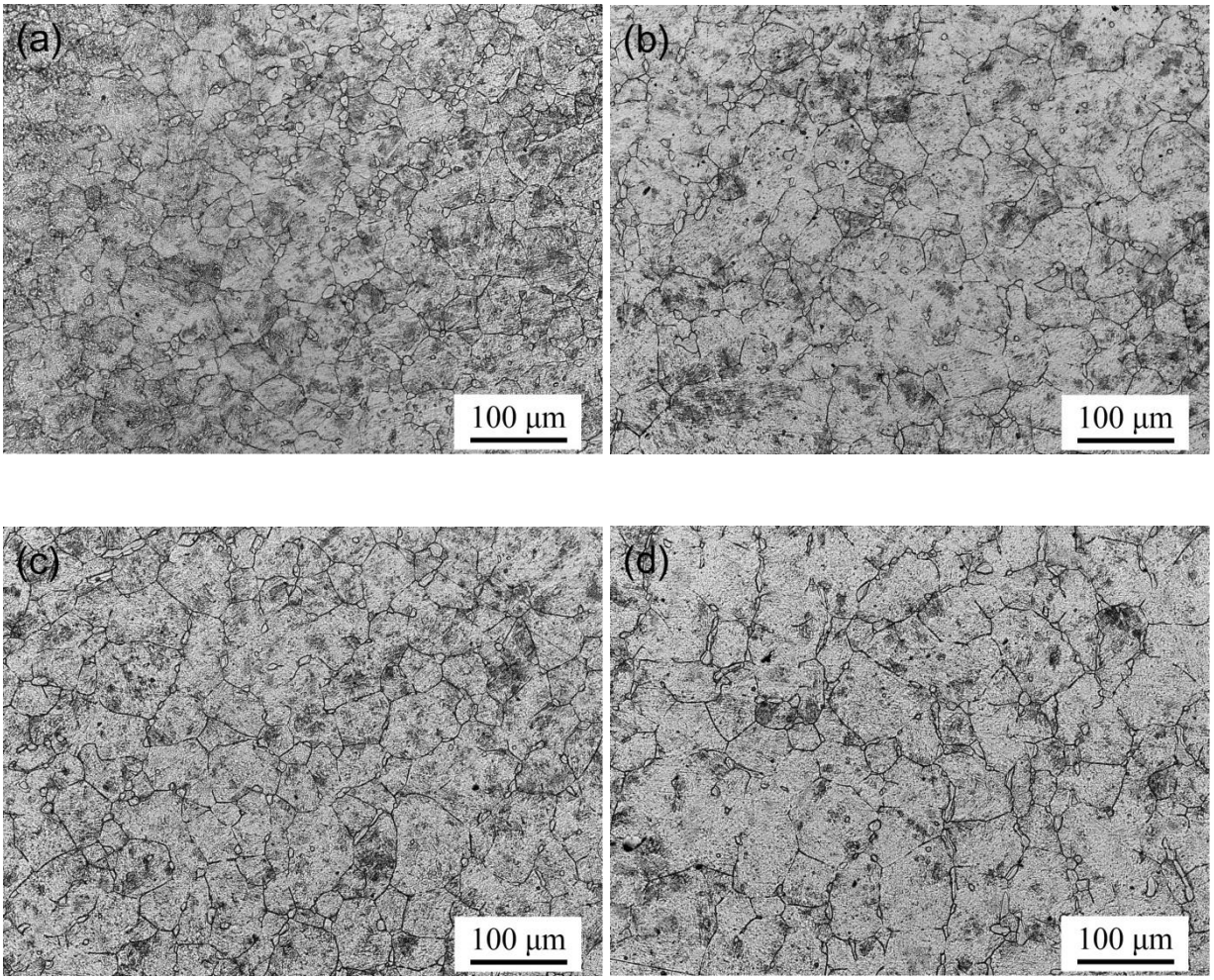

Figure 3. OM micrographs showing the prior austenite grain size obtained under different austenitizing temperatures for 20 minutes, (a) 950 ºC, (b) 1000 ºC, (c) 1050 ºC, (d) 1100 ºC.

Fig. 4 shows the average values of the prior austenite grain size of the high Cr ferritic/martensitic steels at different austenitizing temperatures. The prior austenite grain sizes were measured by the linear intercept method along the horizontal, vertical and 45-degree oblique directions in the figure [19]. The measurement results show that the prior austenite grain size increases from 28 μm to 52 μm with the increase of austenitizing temperature from 950 ºC to 1100 ºC.

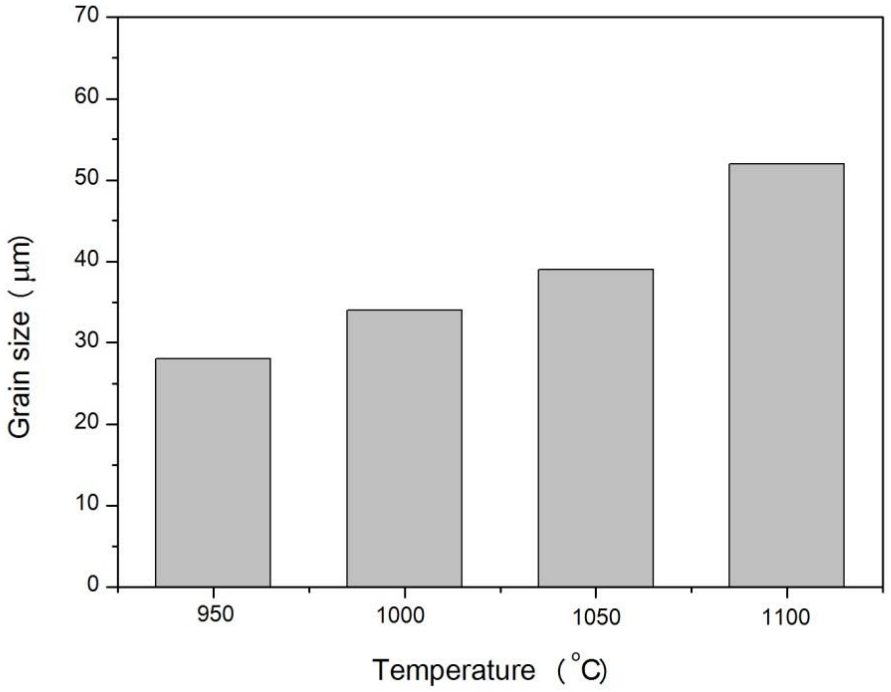

Figure 4. Prior austenite grain size of the high Cr ferritic/martensitic steel subjected to austenitizing temperature from 950 ºC to 1100 ºC.

3.1.2 SEM observation

Since the high Cr ferritic/martensitic steel is normalized + high-temperature tempered during service, the steels with different austenitizing temperatures are tempered. Fig. 5 presents the SEM photographs of the high Cr ferritic/martensitic steels tempered at 750 ºC for 90 minutes after different austenitizing temperatures. It can be seen from the figure that the microstructure of the steels is tempered martensite, and the prior austenite grain size of the matrix does not change significantly before and after tempering. At the same time, it is also found that a large number of precipitates appear along the grain boundaries and lath boundaries after tempering treatment.

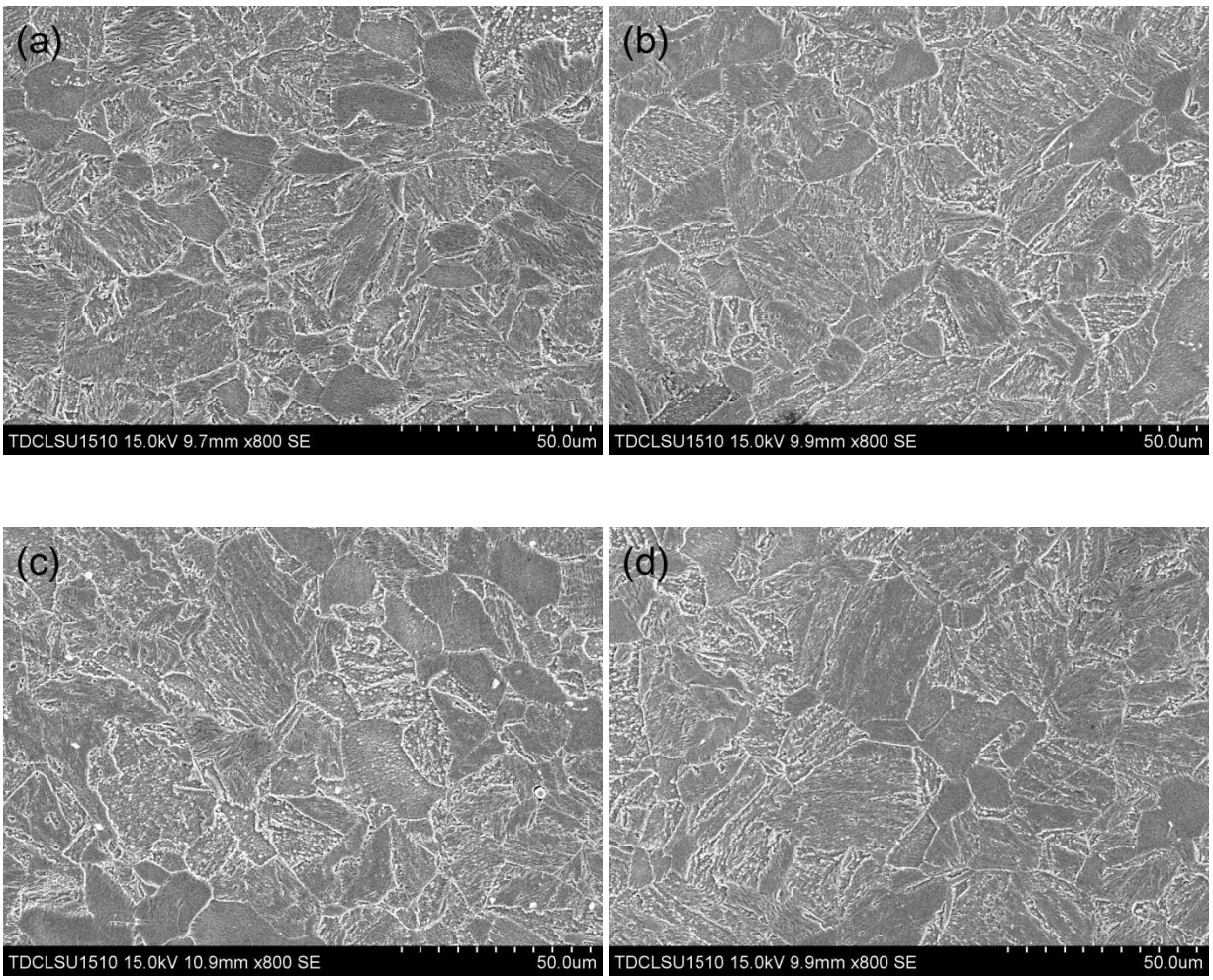

Figure 5. SEM micrographs of the high Cr ferritic/martensitic steels tempered at 750 ^{o}C for 90 minutes after different austenitizing temperatures for 20 minutes, (a) 950 ^{o}C, (b) 1000 ^{o}C, (c) 1050 ^{o}C, (d) 1100 ^{o}C

3.1.3 TEM observation

Aimed at investigating the microstructural evolutions of the steel more clearly, the steels were observed by TEM. Fig. 6 shows the TEM photographs of metal thinning specimens of the high Cr ferritic/martensitic steels tempered at 750 ^{o}C for 90 minutes after different austenitizing temperatures. As can be seen from the figure, there are precipitates on the lath boundaries, and the width of the lath increases significantly with the increase of austenitizing temperature. Y-junctions appear at lower austenitizing temperature (950 ^{o}C and 1000 ^{o}C), which indicates that the lower the austenitizing temperature, the worse the thermal resistance to tempering. This is because a lower austenitizing temperature results in a lower martensitic transformation temperature range. A similar report was also reported in the study of Zhou et al [20].

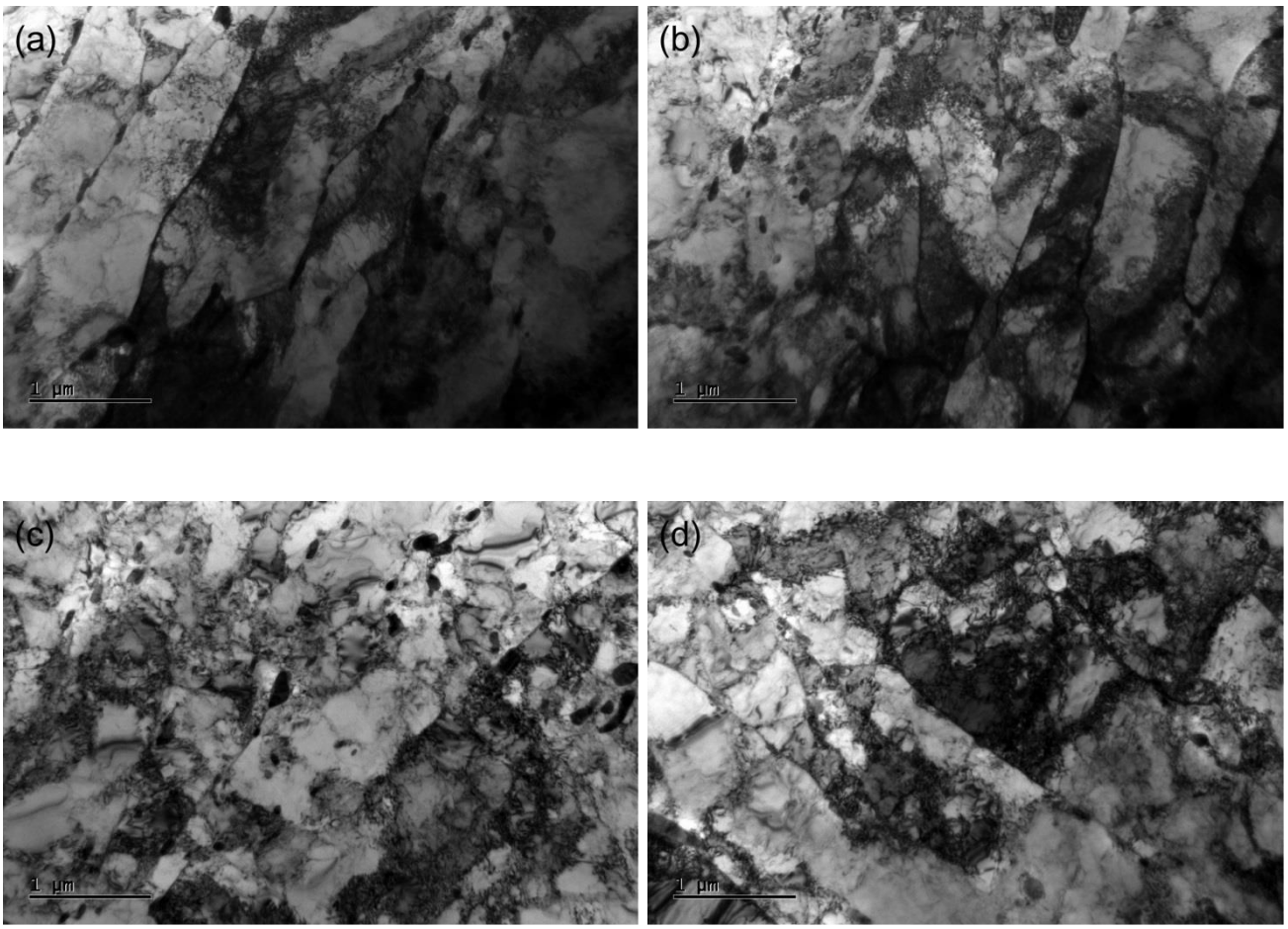

Figure 6. TEM micrographs of metal thinning samples for the high Cr ferritic/martensitic steels tempered at 750 ºC for 90 minutes after different austenitizing temperatures for 20 minutes, (a) 950 ºC, (b) 1000 ºC, (c) 1050 ºC, (d) 1100 ºC

Fig. 7 shows the average width of martensitic lath of tempered high Cr ferritic/martensitic steels after different austenitizing temperatures. The width of martensitic lath is statistically measured along the direction perpendicular to the length of lath by the linear intercept method [21]. The results show that the width of the martensitic lath increases from 380 nm to 600 nm as the austenitizing temperature increases from 950 ºC to 1100 ºC.

Fig. 8 shows the TEM photographs of carbon extraction replica specimens of the high Cr ferritic/martensitic steels tempered at 750 ºC for 90 minutes after different austenitizing temperatures. The distribution of the precipitates is clearly shown. Spherical and granular precipitates are distributed along the prior austenite grain boundaries and martensite lath boundaries due to the high interfacial energy at the boundaries. With the increase of austenitizing temperature, the size of the precipitates first decreases and then increases. It can be confirmed by the EDS analysis in Fig. 8 (e) that the precipitated phases are mainly Cr rich carbides. As a diffusion channel, the boundary is conducive to the diffusion of Cr, thereby promoting the formation of Cr rich carbides [22].

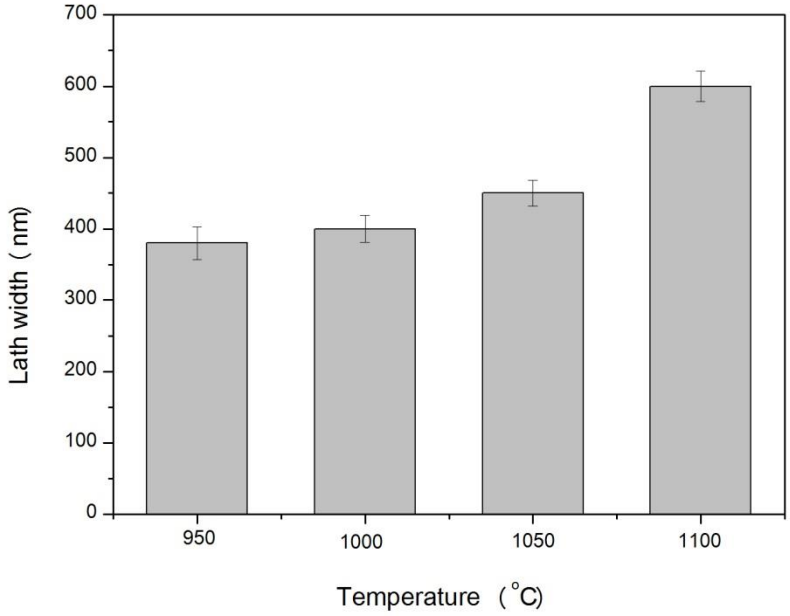

Figure 7. Martensitic lath width of the tempered high Cr ferritic/martensitic steels after austenitizing temperature from 950 ºC to 1100 ºC.

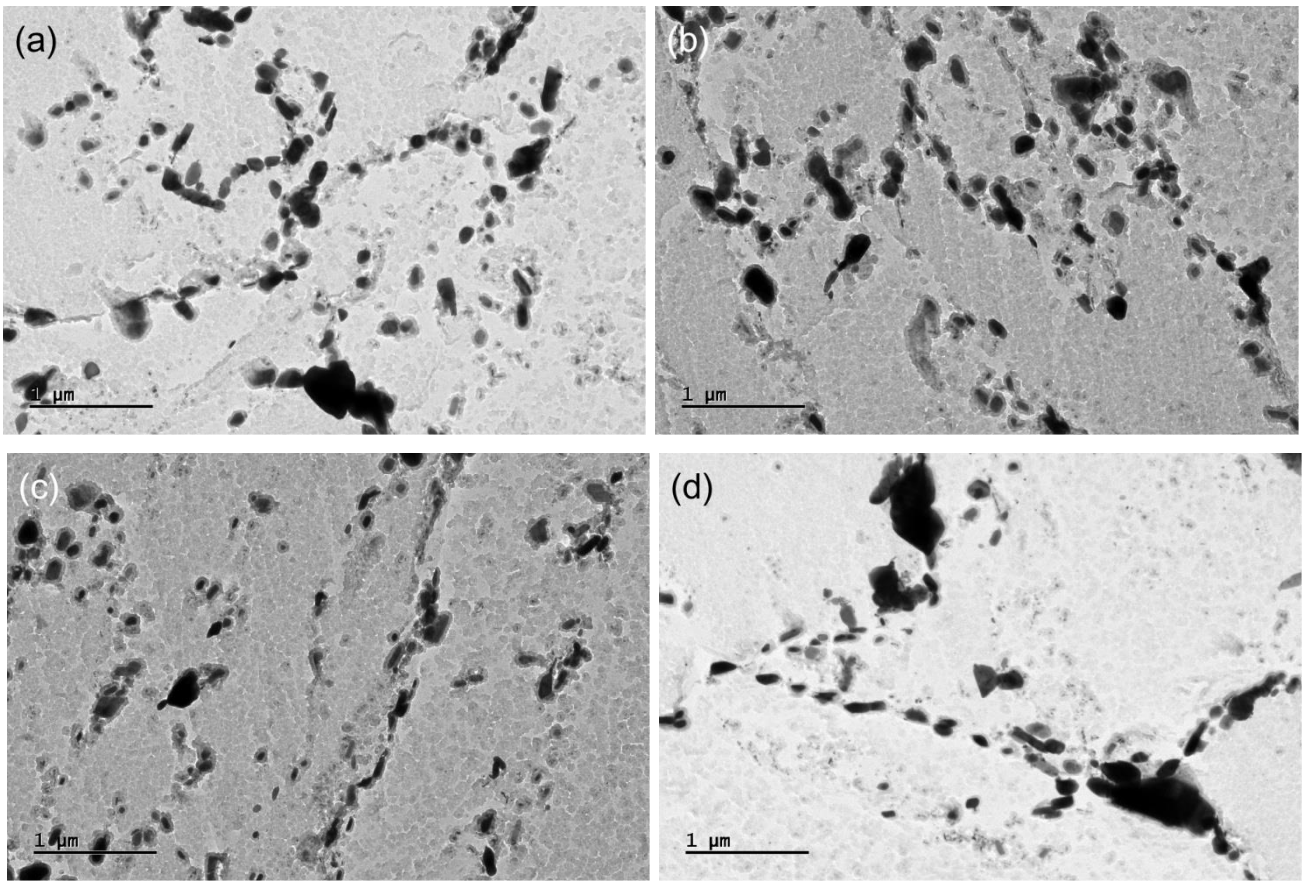

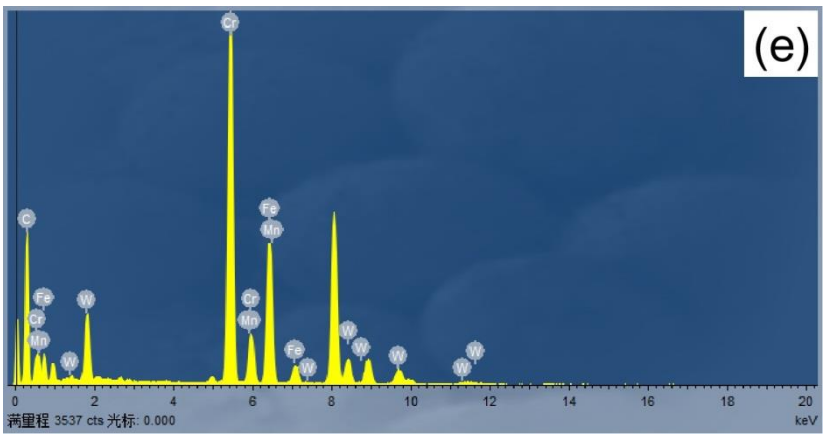

Figure 8. TEM micrographs of extraction replica samples for the high Cr ferritic/martensitic steels tempered at 750 ºC for 90 minutes after different austenitizing temperatures for 20 minutes, (a) 950 ºC, (b) 1000 ºC, (c) 1050 ºC, (d) 1100 ºC, (e) EDS analysis of carbide.

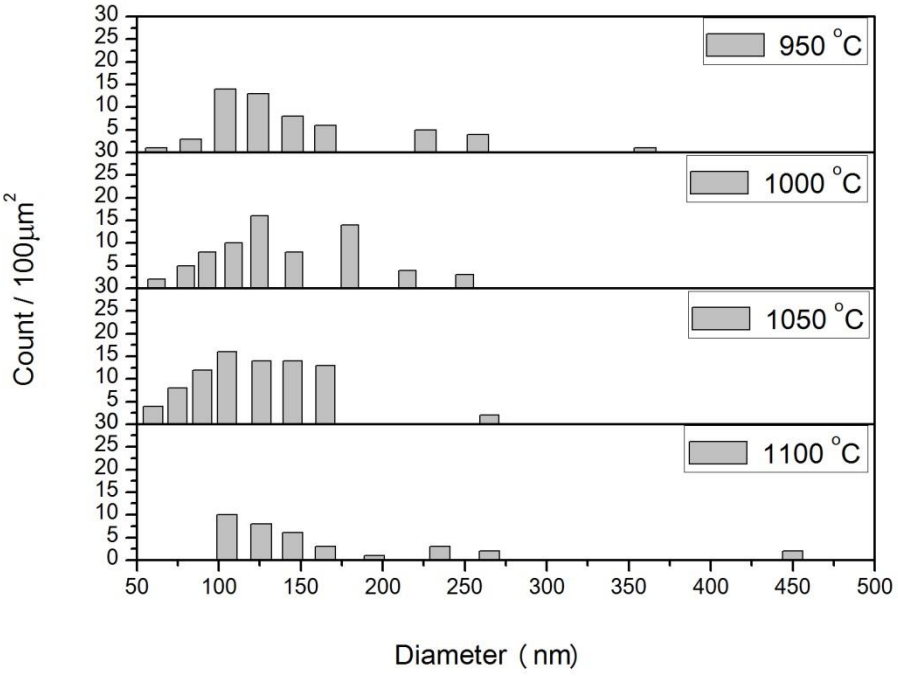

Figure 9. Density and size of carbide in the high Cr ferritic/martensitic steels tempered at 750 ºC for 90 minutes after austenitizing temperature from 950 ºC to 1100 ºC

In order to quantify the distribution of the Cr rich carbides in the high Cr ferritic/martensitic steels tempered at at 750 ºC for 90 minutes after different austenitizing temperatures, the size and quantity of carbides in the steels subjected to different austenitizing temperatures were counted, as shown in Fig. 9. Each quantitative statistic result is obtained by counting multiple TEM micrographs. It can be seen from the figure that the number of the carbides in the tempered steel first increases and then decreases with the increase of austenitizing temperature, while the size of the carbides first decreases and then increases with the increase of austenitizing temperature. The turning point is the

austenitizing temperature of 1050 ºC. At the lower austenitizing temperatures (950 ºC and 1050 ºC), there are more primary undissolved carbides in the steel. These undissolved carbides can be used as the nucleation position of new carbide particles in the tempering process, resulting in the formation of large carbide particles. Since all specimens were tempered at 750 ºC for 90 minutes, the total fraction of carbide particles in the four specimens was approximately the same. When the austenitizing temperature is 1100 ºC, the density of carbides in the tempered steel is the smallest, so its size is the largest [23].

3.2 Corrosion resistance of the high Cr ferritic/martensitic steels

3.2.1 Electrochemical analysis

Fig. 10 shows the electrochemical polarization curves of the high Cr ferritic/martensitic steels tempered at 750 ºC for 90 minutes after different austenitizing temperatures in 3.5 wt.% NaCl solution. It can be seen that the shape and changing trend of the polarization curves of the tempered steels after different austenitizing temperatures are similar. The corrosion potential (Ecorr) can be read directly on the polarization curves. The corrosion current density (icorr) for each specimen was calculated by Tafel extrapolation of the anode and cathode branches of the polarization curves [24]. Table 2 lists the electrochemical parameters (Ecorr and icorr) of the tempered high Cr ferritic/martensitic steels after different austenitizing temperatures. It can be seen from the data in the table that the icorr of the specimen first decreases and then increases with the increase of austenitizing temperature. The change range of Ecorr is very small, which shows the opposite change trend with icorr.

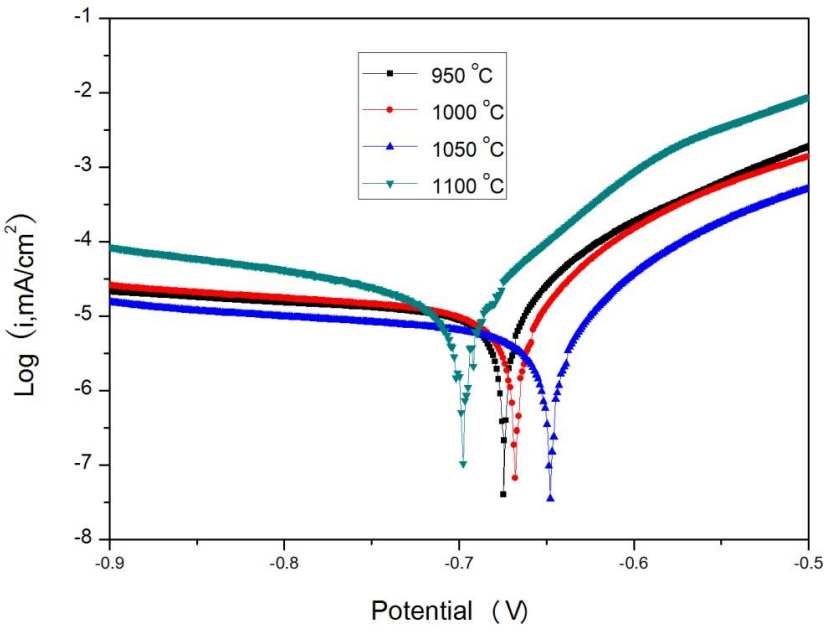

Figure 10. Electrochemical polarization curves of the high Cr ferritic/martensitic steels tempered at 750 ºC for 90 minutes after austenitizing temperature from 950 ºC to 1100 ºC.

Table 2. Electrochemical parameters of the high Cr ferritic/martensitic steels tempered at 750 ºC for 90 minutes after austenitizing temperature from 950 ºC to 1100 ºC in 3.5 wt.% NaCl solution

Auustenitizing Temperature (ºC)	E_{corr} (V)	I_{corr} (μA/cm^2)
950	-0.674	3.84
1000	-0.668	3.78
1050	-0.648	3.52
1100	-0.698	4.22

Although the icorr can represent the corrosion resistance of steel, the corrosion rate is the most intuitive parameter to describe the corrosion resistance of the high chromium ferritic/martensitic steel. It can be calculated by the following formula [25]:

$$\text{Corrosion rate} = \frac{3.27 \times i_{corr} \times \text{A}}{\text{nD}} \quad (1)$$

Where A is the atomic weight, n is the number of electrons exchanged in the electrochemical reaction, and D is the density of the material.

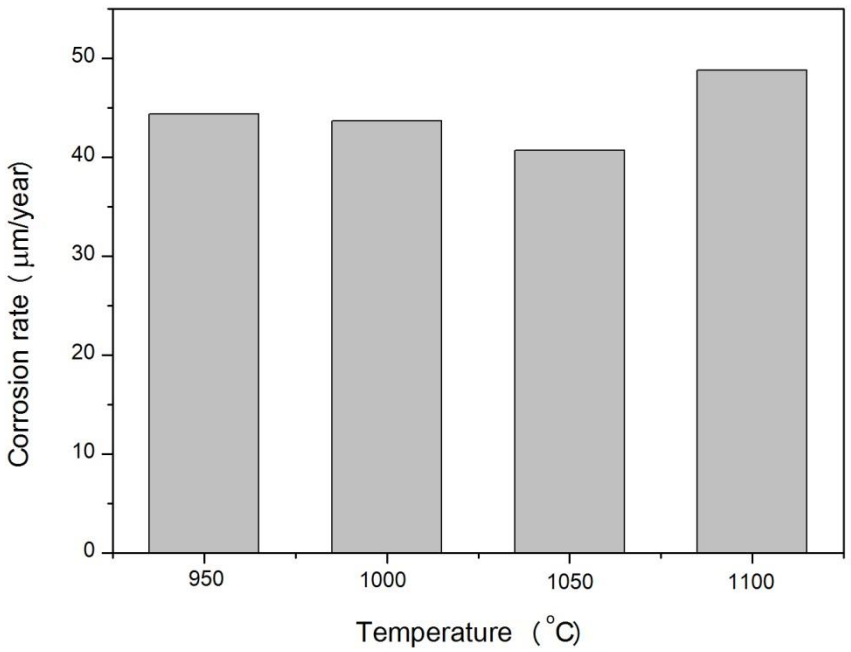

Figure 11. Corrosion rate of the high Cr ferritic/martensitic steels tempered at 750 ºC for 90 minutes after austenitizing temperature from 950 ºC to 1100 ºC.

For the corrosion rate calculation of iron-based metallic materials [26], A can be chosen to be the atomic weight of iron (A = 55.84), D can be chosen as the density of iron (D = 7.90 g/cm^3), and the

value of n is 2. Fig. 11 shows the corrosion rates of the high Cr ferritic/martensitic steels tempered at 750 ºC for 90 minutes after austenitizing temperature from 950 ºC to 1100 ºC. There is a good correspondence between the corrosion rate and the icorr obtained from the polarization curve. As the austenitizing temperature increased from 950 ºC to 1050 ºC, the corrosion rate decreased from 44.4 μm/year to 40.7 μm/year. The austenitizing temperature was further increased to 1100 ºC, and the corrosion rate increased to 48.8 μm/year.

3.2.2 Corrosion mechanism

The reason for the variation in corrosion resistance of the tempered high Cr ferritic/martensitic steels after different austenitizing temperatures can be attributed to the Cr rich carbides in the matrix. A previous study confirmed that the formation of Cr rich carbides consumes Cr in the matrix and reduces the formation of surface passive film [27]. In addition, there is a phase potential difference between the Cr rich carbides and the matrix, forming a localized galvanic couple [28]. Furthermoer, the more inhomogeneous the distribution of Cr rich carbides, the more likely it is to form localized galvanic couples in the whole matrix. The larger the local galvanic couple, the worse the corrosion resistance [29]. Cr rich carbides segregated along the grain boundaries at low austenitizing temperatures (950 ºC and 1000 ºC) are difficult to dissolve, and will act as the nucleation sites of the newly precipitated Cr rich carbides along grain boundaries and lath boundaries during the subsequent tempering, which leads to the formation of large-sized Cr rich carbides [30]. The concentration of Cr elements forming large-sized Cr rich carbides is greater than that in the matrix around the flanks and in the adjacent grain boundaries, resulting in the formation of Cr depleted regions, which in turn reduce the corrosion resistance at these locations [31-34]. The increase of austenitizing temperature from 950 ºC to 1050 ºC leads to the dissolution of undissolved carbides and the uniform distribution of elements, which can enhance the pitting corrosion resistance of steel [35-37]. Under the austenitizing condition of 1100 ºC, the larger Cr rich carbides are precipitated at the grain boundaries and lath boundaries during subsequent tempering, resulting in an increase in the extent of the Cr depleted regions, thereby reducing the corrosion resistance. In addition, larger carbide particles can lead to a lower pitting potential and deteriorate the corrosion resistance of steel [38].

4. CONCLUSIONS

In this paper, the effects of austenitizing temperature on the microstructure evolution and corrosion resistance of the high Cr ferritic/martensitic steel have been studied. The main conclusions are as follows:

(1) The prior austenite grain size of the high Cr ferritic/martensitic steel increases from 28 μm to 52 μm with the increase of austenitizing temperature from 950 ºC to 1100 ºC.

(2) As the austenitization temperature increases from 950 ºC to 1100 ºC, the martensitic lath width of the high Cr ferritic/martensitic steel increases from 380 nm to 600 nm.

(3) The carbide size in the steel becomes smaller and its density becomes larger when the

austenitizing temperature increases from 950 ºC to 1050 ºC. However, when the austenitizing temperature increases from 1050 ºC to 1100 ºC, the carbide size and density show an opposite trend to changes in carbides below 1050 ºC.

(4) With the increase of austenitizing temperature, the corrosion current density of the high Cr ferritic/martensitic steel first decreases and then increases, and the corrosion potential first increases and then decreases.

(5) As the austenitization temperature increases from 950 ºC to 1100 ºC, the corrosion resistance of the steel first increases and then deteriorates. The corrosion rate decreases from 44.4 μm/year to 40.7 μm/year when the austenitizing temperature was increased from 950 ºC to 1050 ºC, however, it increased to 48.8 μm/year when the austenitizing temperature was increased from 1050 ºC to 1100 ºC.

ACKNOWLEDGEMENTS
This work was financially supported by the Science and Technology Program of Tianjin Administration for Market Regulation (No. 2017-W30).

CONFLICTS OF INTEREST
The authors declare that they have no known competing financial interests that could have appeared to influence the work reported in this paper.

DATA AVAILABILITY STATEMENT
All data generated or analyzed during this work are included within the article.

References

1. J.G. Chen, Y.C. Liu, Y.T. Xiao, Y.H. Liu, C.X. Liu and H.J. Li, *Acta Metall. Sin. (Engl. Lett.)*, 31 (2018) 706. https://doi.org/10.1007/s40195-018-0703-y
2. X. Zhou, Y. Liu, C. Liu and B. Ning, *Mater. Sci. Eng. A* 608 (2014) 46. https://doi.org/10.1016/j.msea.2014.04.075
3. H. He, L. Yu, C. Liu, H. Li, Q. Gao and Y. Liu, *Acta Metall. Sin.*, 58 (2022) 311. https://doi.org/ 10.11900/0412.1961.2021.00185
4. J.G. Chen, C.X. Liu, C. Wei, Y.C. Liu and H.J. Li, *Acta Metall. Sin. (Engl. Lett.)*, 32 (2019) 1151. https://doi.org/ 10.1007/s40195-019-00883-6
5. X. Zhou, C. Liu, L. Yu, Y. Liu and H. Li, *J. Mater. Sci. Technol.*, 31 (2015) 235. https://doi.org/10.1016/j.jmst.2014.12.001
6. Z. Xia, C. Zhang, H. Lan and Z. Yang, *J. Mater. Sci.*, 46 (2011) 3151. https://doi.org/10.1007/s10853-010-5196-7
7. C. Liu, C. Mao, L. Cui, X. Zhou, L. Yu, and Y. Liu, *Acta Metall. Sin.*, 57 (2021) 1521. https://doi.org/10.11900/0412.1961.2021.00348
8. J.G. Chen, C.X. Liu, C. Wei, Y.C. Liu and H.J. Li, *J. Manuf. Process.*, 43 (2019) 192. https://doi.org/10.1016/j.jmapro.2019.05.020
9. X.S. Zhou, Y.C. Liu, Z.X. Qiao, Q.Y. Guo, C.X. Liu, L.M. Yu and H.J. Li, *Fusion Eng. Des.*, 125

(2017) 354.
https://doi.org/10.1016/j.fusengdes.2017.05.095
10. J.G. Chen, Y.C. Liu, C.X. Liu, B.Y. Yan and H.J. Li, *J. Iron Steel Res. Int.*, 24 (2017) 705.
https://doi.org/10.1016/s1006-706x(17)30106-1
11. J. Vivas, C. Capdevila, E. Altstadt, M. Houska and D.San-Martín, *Scripta Mater.*, 153 (2018) 14.
https://doi.org/10.1016/j.scriptamat.2018.04.038
12. Q.Z. Gao, Y.C. Liu, X.J. Di, L.M. Yu, Z.S. Yan and Z.X. Qiao, *Nucl. Eng. Des.*, 256 (2013) 148.
https://doi.org/10.1016/j.nucengdes.2012.12.009
13. C.L. Mao, C.X. Liu, L.M. Yu, H.J. Li and Y.C. Liu, *Mater. Sci. Eng*. A, 739 (2019) 90.
https://doi.org/ 10.1016/j.msea.2018.10.023
14. X. Zhou, G. Liu, X. Shen, and Y. Liu, *Mater. Sci. Eng*. A, 829 (2022) 142071.
https://doi.org/ 10.1016/j.msea.2021.142071
15. C. Pandey, A. Giri, M.M. and Mahapatra, *Mater. Sci. Eng.* A, 657 (2016) 173.
https://doi.org/10.1016/j.msea.2016.01.066
16. P. Yan, Z. Liu, H. Bao, Y. Weng, and W. Liu, *Mater. Sci. Eng. A*, 597 (2014) 148.
https://doi.org/10.1016/j.msea.2013.12.068
17. C. Wei, Z.J. Wang and J.G. Chen, *Eng. Fail. Anal.*, 135 (2022) 106111.
https://doi.org/10.1016/j.engfailanal.2022.106111
18. S. Morito, H. Saito, T. Ogawa, T. Furuhara and T. Maki, *ISIJ. Int.*, 45 (2005) 91.
https://doi.org/10.2355/isijinternational.45.91
19. J.G. Chen, Y.C. Liu, C.X. Liu, X.S. Zhou and H.J. Li, *J. Mater. Res.*, 32 (2017) 1376.
https://doi.org/10.1557/jmr.2017.77
20. X.S. Zhou, Y.C. Liu, C.X. Liu, L.M. Yu and H.J. Li, *Metall. Mater. Trans.* A, 49 (2018) 3525.
https://doi.org/10.1007/s11661-018-4723-z
21. J.G. Chen, C.X. Liu, Y.C. Liu, B.Y. Yan and H.J. Li, *J. Nucl. Mater.*, 479 (2016) 295.
https://doi.org/10.1016/j.jnucmat.2016.07.029
22. W. Yan, W. Wang, Y. Shan, K. Yang, and W. Sha, 9-12Cr Heat-resistant steels, Springer, Switzerland, (2015) pp. 121-122.
https://doi.org/10.1007/978-3-319-14839-7_6
23. Z. Liu, X.J. Huo, Y.H. Yu, C. Zhang, N. Xiao, J.L. Zhao and Z.G. Yang, *Mater. Sci. Eng.* A, 826 (2021) 141934.
https://doi.org/ 10.1016/j.msea.2021.141934
24. C. Wei, Y.S. Wei, Z.J. Wang and J.G. Chen, *Int. J. Electrochem. Sci.*, 17 (2027) 220622.
https://doi.org/10.20964/2022.06.02
25. D.Song, J. Hao, F. Yang, H. Chen, N. Liang, Y. Wu, J. Zhang, H. Ma, E.E. Klu, B. Gao, Y. Qiao, J. Sun and J. Jiang, *J. Alloy. Compd.*, 809 (2019) 151787.
https://doi.org/10.1016/j.jallcom.2019.151787
26. J.G. Chen, Y.M. Yang, L.Q. Li, Z.J. Wang, H.Y. Xiao, Y.S. Wei, T.H. Zhu and H. Song, *Int. J. Electrochem. Sci.*, 16 (2021) 210825.
https://doi.org/10.20964/2021.08.36
27. R. Li, B.G. Fu, T.S. Dong, G.L. Li, J.K. Li, X.B. Zhao and J.H. Liu, *J. Mater. Res. Technol.*, 18 (2022) 448.
https://doi.org/10.1016/j.jmrt.2022.02.117
28. H. Wan, Y. Cai, D. Song and C. Chen, *Corros. Sci.*, 167 (2020) 108518.
https://doi.org/10.1016/j.corsci.2020.108518
29. R. Yuan, X. Yu, Y. Zhang, H. Wu and H. Guo, *Mater.Today Commun.*, 31 (2022) 103715.
https://doi.org/10.1016/j.mtcomm.2022.103715
30. Z. Xia, C. Zhang, Q. Huang, S. Liu, Z. Li and Z. Yang, *J. Iron Steel Res. Int.*, 18 (2011) 47.
https://doi.org/10.1016/S1006-706X(12)60033-8
31. S. Zhang, H. Li, Z. Jiang, B. Zhang, Z. Li, J. Wu, S. Fan H. Feng and H. Zhu, *Mater. Charact.*, 152

(2019) 141.
https://doi.org/10.1016/j.matchar.2019.04.010
32. S. Hu, Y. Mao, X. Liu, E. Han and H. Hänninen, *Corros. Sci.*, 166 (2020) 108420.
https://doi.org/10.1016/j.corsci.2019.108420
33. X.L. Li, L.T. Chang, C.P. Liu, B. Leng, X.X. Ye, F.F. Han and X.M. Yang, *Corros. Sci.*, 191 (2021) 109784.
https://doi.org/10.1016/j.corsci.2021.109784
34. S. Salahi, M. Ghaffari, A.V. Nemani and A. Nasiri, *J. Mater. Eng. Perform.*, 30 (2021) 6618.
https://doi.org/10.1007/s11665-021-05936-5
35. Y.S. Choi, J.G. Kim, Y.S. Park and J.Y. Park, *Mater. Lett.*, 61 (2007) 244.
https://doi.org/10.1016/j.matlet.2006.04.041
36. H.B. Liu, W.C. Jiao, H. Feng, Z.H. Jiang and C.D. Ren, *Acta Metall. Sin. (Engl. Lett.)*, 29 (2016) 1148.
https://doi.org/ 10.1007/s40195-016-0506-y
37. S.Y. Lu, K.F. Yao, Y.B. Chen, M.H. Wang, Y. Shao and X.Y. Ge, *J. Appl. Electrochem.*, 45 (2015) 375.
https://doi.org/10.1007/s10800-015-0796-1
38. H.Y. Li, C.F. Dong, K. Xiao, X.G. Li and P. Zhong, *Acta Metall. Sin. (Engl. Lett.)*, 29 (2016) 1064.
https://doi.org/ 10.1007/s40195-016-0481-3